

# Inerter-based Elastic Metamaterials for Band Gap at Extremely Low Frequency

Faisal Jamil,<sup>1</sup> Fei Chen,<sup>1</sup> Bolei Deng,<sup>2</sup> Robert G. Parker,<sup>1</sup> and Pai Wang<sup>1</sup>

<sup>1</sup>*Department of Mechanical Engineering, University of Utah, Salt Lake City, UT, USA*

<sup>2</sup>*Computer Science and Artificial Intelligence Laboratory,*

*Department of Electrical Engineering and Computer Science, and Department of Mechanical Engineering, Massachusetts Institute of Technology, Cambridge, MA, USA*

We reveal the unique and fundamental advantage of inerter-based elastic metamaterials by a comparative study among different configurations. When the embedded inerter is connected to the matrix material on both ends, the metamaterial shows definite superiority in forming a band gap in the ultra-low frequency - equivalently the ultra-long wavelength - regime, where the unit cell size can be four or more orders of magnitude smaller than the operating wavelength. In addition, our parametric studies in both one and two dimensions pave the way towards designing next-generation metamaterials for structural vibration mitigation.

Mitigation of low-frequency vibrations has long been a major challenge. One promising research direction points to architected materials - widely referred to as acoustic or elastic metamaterials [1–6]. They can exhibit a phononic band gap, i.e., a range of frequencies in which no vibration can propagate. While many recent studies attempted to demonstrate low-frequency band gaps [7–32], there is no consensus on which frequency ranges should be called “low” or “ultra-low”. The exact meaning of low frequency varies from a fraction of one Hz [12, 21], to several Hz [7, 8, 20], and up to many kHz [11, 23, 28]. The word “low” is a relative concept that depends on application-specific scenarios.

To facilitate a generally meaningful discussion and a fair comparison among different systems and configurations, here we focus on a universal and dimensionless frequency for all vibro-elastic metamaterials:  $f = a/\lambda$ , where  $a$  denotes the size of a metamaterial unit, and  $\lambda$  is the operating wavelength. All scattering-based band gaps in phononic crystals [33, 34] are at the order of  $f = a/\lambda \sim 1$ . In contrast, locally resonant metamaterials embedded with mass-resonators [35, 36] usually exhibit band gaps at a much lower frequency range of  $f = a/\lambda \sim 10^{-2}$  to  $10^{-3}$ .

In this Letter, we demonstrate the unique capability of inerter-based metamaterials in forming band gaps at the ultra-low dimensionless frequencies, where  $f = a/\lambda \sim 10^{-4}$ . The key component is the inerter, a two terminal mechanical device offering a *frequency-independent* inertia much larger than its own physical mass [37, 38]. As illustrated in Fig. 1, this is possible because the inerter couples linear relative motions between its two ends to the rotation of a flywheel. The flywheel moment of inertia can be amplified to produce a large inertial effect. The use of rotational motion also makes it possible for the device to be compact. Like springs and dampers, the inerter is a passive device without the need of any active control. As shown in Fig. 1(a), the inerter’s behavior is characterized by the response force,  $F = b(\ddot{u}_1 - \ddot{u}_2)$ , where  $\ddot{u}_1$  and  $\ddot{u}_2$  are the accelerations

at the two terminals. The constant  $b$  is called the inertance, which has the same unit as mass. The performance attributes of inerters have been experimentally verified with ball-screw designs [37, 39–44], rack-pinion designs [37, 39, 40, 45], and hydraulic designs [46, 47]. Their basic structures are shown in Figs. 1(b), 1(c) and 1(d), respectively. In particular, the hydraulic inerter design benefits from the small physical mass of nearly incompressible fluid that fills the inerter, so that it can produce an inertance that is  $1.5 \times 10^6$  times larger than its own the physical mass [47].

While there have been several pioneering attempts to incorporate inerters into metamaterial designs [48–54]. A critical study to identify and overcome the fundamental hurdles is still missing. With theoretical and numerical analyses of different designs, we investigate the basic challenges and offer a road map to realize vibration-band-gap metamaterials with unit cells in the ultra-deep sub-wavelength scale of  $a/\lambda \sim 10^{-4}$ .

To start, we model any matrix material or base structure of metamaterials as a spring-mass chain with stiffness  $K$  and point mass  $M$ , as shown in Fig. 2(a). This model is valid since we aim at the long-wavelength limit of  $\lambda \gg a$ , where the discrete nature of the main chain has

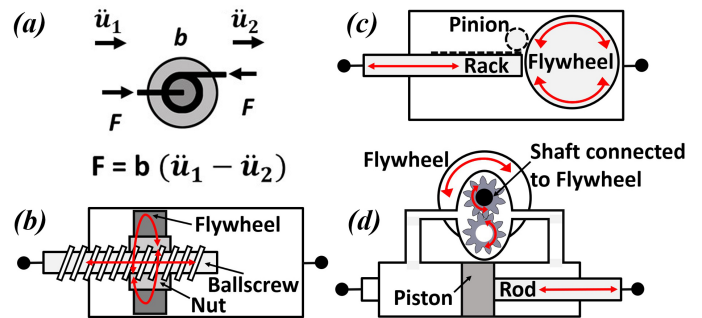


FIG. 1. Conceptual schematics of inerters: (a) Abstract symbol and force response. (b) Ball-screw inerter. (c) Rack-and-pinion inerter. (d) Hydraulic inerter.

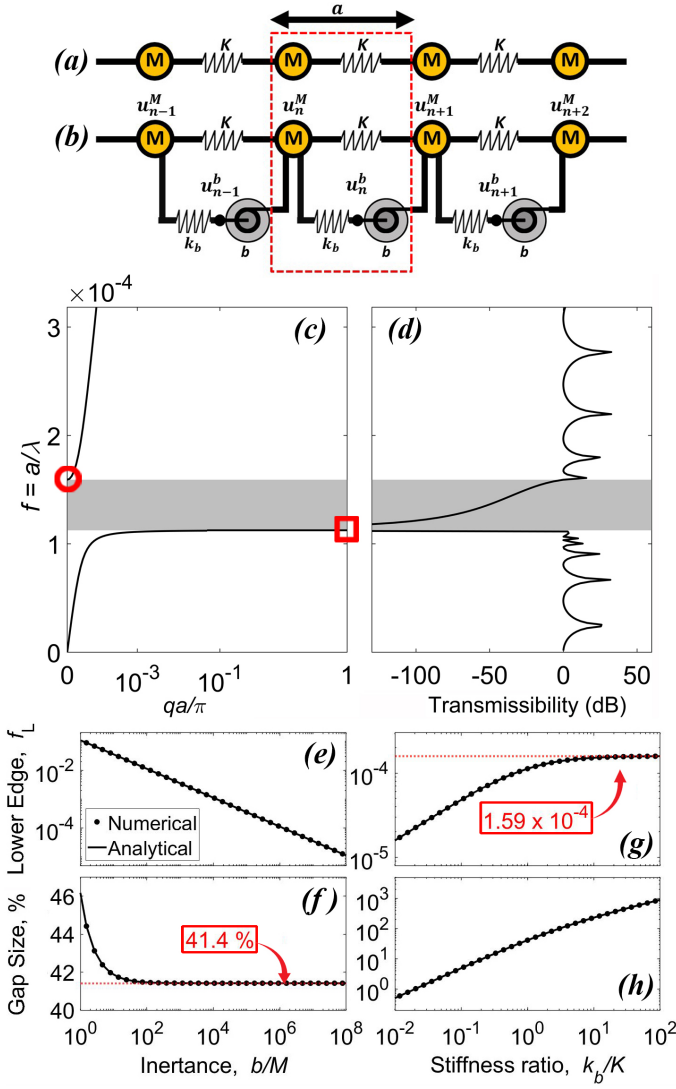


FIG. 2. Discrete models and band gaps: (a) Abstraction of any matrix material as a spring-mass chain; (b) Inerter-based metamaterial; (c) Dispersion curves and band gap (shaded region) of inerter-based metamaterial shown in (b) with  $b/m_b = b/M = 10^6$  and  $k_b/K = 1$ ; and (d) Finite-chain response of inerter-based metamaterial with 1000 unit cells. The transmissibility is calculated as the ratio between output and input amplitudes. Parametric studies on the band gap lower edge frequency and relative size: (e) and (f) show the effects of change in the inertia ratio,  $\mu_b = b/M$ , with fixed  $\kappa_b = k_b/K = 1$ . (g) and (h) show the effects of change in the stiffness ratio,  $\kappa_b = k_b/K$ , with fixed  $\mu_b = b/M = 10^6$ .

negligible impact on the results. With this setup, we can normalize all metamaterial dispersion relations according to the main-chain wave speed in the long-wavelength limit,  $c = a\sqrt{K/M}$ , so that all band gap frequencies are non-dimensionalized [1, 38] as  $f = \omega a/(2\pi c) = a/\lambda$ , where  $\omega$  is the dimensional angular frequency in metamaterial dispersion relations.

We analyze three types of metamaterial designs

with: embedded inerters [48, 49, 52, 53], inerter-mass-resonators [48–52, 54, 55], and traditional mass-resonators [35, 36], as shown in Figs. 2(b), 4(a) and 4(b), respectively. Applying the Bloch theorem [2, 38], we calculate the dispersion relations of each system and investigate their behaviors at the low-frequency limit.

First, we consider metamaterials with the embedded inerter and no other additional mass, as illustrated in Fig. 2(b). The model has two degrees of freedom in the unit cell:  $u^M$  - displacement of mass  $M$  on the main chain and  $u^b$  - displacement of the point between stiffness  $k_b$  and inerter  $b$  on the side chain. With the parameters  $k_b/K = 1$  and  $b/M = 10^6$ , the dispersion relation plotted in Fig. 2(c) shows a band gap as the grey-shaded range near  $f = a/\lambda \sim 10^{-4}$ . The horizontal axis of normalized wave number  $qa/\pi$  is shown in logarithmic scale because the band-gap effects happen at very long wavelength. This ultra-low frequency band gap is further demonstrated by transmission attenuation in the steady-state dynamics simulation of a finite chain [38], with results shown in Fig. 2(d). The band gap's lower edge frequency,  $f_L$ , is the eigen-frequency of the first band at  $q = \pi/a$ , as labelled by a red square in Fig. 2(c). Similarly, the band gap's upper edge frequency,  $f_U$ , is the eigen-frequency of the second band at  $q = 0$ , as labelled by a red circle in Fig. 2(c). As good non-dimensionalized measures for comparison purposes, we characterize the band gap by two quantities: (1) The starting dimensionless frequency,  $f_L$ ; and (2) The relative gap size  $\Delta f = (f_U - f_L)/f_L$ . Fig. 2(e) shows the numerical results as  $f_L = 1.125 \times 10^{-4}$  with a relative gap size of  $\Delta f \approx 41.4\%$ .

More generally, we can obtain the analytical equations,

$$f_L = \frac{1}{2\pi} \sqrt{\chi_b - \sqrt{\chi_b^2 - 4\frac{\kappa_b}{\mu_b}}} \quad \text{and} \quad f_U = \frac{1}{2\pi} \sqrt{\frac{\kappa_b}{\mu_b}}, \quad (1)$$

where  $\chi_b = 2\kappa_b + \kappa_b/(2\mu_b) + 2$ ,  $\kappa_b = k_b/K$ , and  $\mu_b = b/M$ . These closed-form results enable us to perform asymptotic convergence analyses [38]. At the limit of large inertia,  $\mu_b \gg \kappa_b$ , we have

$$f_L \rightarrow \frac{1}{2\pi} \sqrt{\frac{\kappa_b}{\mu_b(\kappa_b + 1)}} \quad \text{and} \quad \Delta f \rightarrow \sqrt{\kappa_b + 1} - 1. \quad (2)$$

These equations reveal a unique advantage of the design with embedded inerters: As the inertia  $b = \mu_b M$  increases, the band gap shifts to a lower frequency. At the same time, the relative gap size,  $\Delta f$ , approaches a finite and low limit, keeping the band gap open at very low frequencies. This convergence is also shown together with numerical results in Figs. 2(e) and 2(f) with  $\kappa_b = k_b/K = 1$ , where the gap size converges to  $\Delta f = \sqrt{2} - 1 \approx 41.4\%$  for large  $\mu_b$ . In the same limit, we can also get the modal displacement ratios at the gap

edges as:

$$\begin{aligned} U^b/U^M &\rightarrow 1 + 2/\kappa_b \quad \text{at } f = f_L, \\ U^b/U^M &\rightarrow 1 \quad \text{at } f = f_U, \end{aligned} \quad (3)$$

where  $U^b$  and  $U^M$  are modal amplitudes of  $u^b$  and  $u^M$ , respectively. Furthermore, taking the additional limit of  $\kappa_b \gg 1$  gives

$$\begin{aligned} f_L &\rightarrow \frac{1}{2\pi} \sqrt{\frac{1}{\mu_b}}, \quad \Delta f \rightarrow \sqrt{\kappa_b}, \\ U^b/U^M &\rightarrow 1 \quad \text{at both } f_L \text{ and } f_U. \end{aligned} \quad (4)$$

This shows that it is beneficial to have stiff connections between the inerter and the main chain: While we can get larger gap size as  $k_b = \kappa_b K$  increases, the gap's starting frequency will saturate and converges to a finite limit, retaining the ultra-low frequency feature with large inertance. This high-stiffness convergence is shown together with numerical results in Figs. 2(g) and 2(h) with  $\mu_b = b/M = 10^6$ . The lower gap edge converges to  $f_L = 10^{-3}/(2\pi) \approx 1.59 \times 10^{-4}$ .

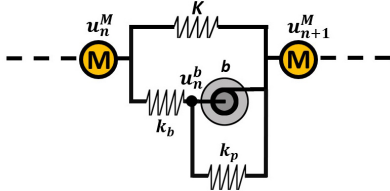


FIG. 3. The unit cell of Inerter-based metamaterial with an additional stiffness,  $k_p$ , parallel to the embedded inerter.

An important variant design involves an additional stiffness,  $k_p$ , parallel to the embedded inerter. As shown in Fig. 3, each unit cell still has two degrees of freedom. We perform the same analyses as before and obtain the equations for both upper and lower edges of the band gap in this case as

$$f_L = \frac{1}{2\pi} \sqrt{\chi_p - \sqrt{\chi_p^2 - \frac{4(\kappa_b + \kappa_b \kappa_p + \kappa_p)}{\mu_b}}}, \quad (5a)$$

$$f_U = \frac{1}{2\pi} \sqrt{\frac{(\kappa_b + \kappa_p)}{\mu_b}}, \quad (5b)$$

where  $\chi_p = 2\kappa_b + (\kappa_b + \kappa_p)/(2\mu_b) + 2$ ,  $\kappa_b = k_b/K$ ,  $\kappa_p = k_p/K$ , and  $\mu_b = b/M$ . At the limit of large inertance ( $\mu_b \gg \kappa_b, \kappa_p$ ) and taking  $\kappa_b = 1$ , we get the asymptotic convergence

$$f_L \rightarrow \frac{1}{2\pi} \sqrt{\frac{2\kappa_p + 1}{2\mu_b}} \quad \text{and} \quad \Delta f \rightarrow \sqrt{1 + \frac{1}{2\kappa_p + 1}} - 1, \quad (6)$$

which indicate that, as the parallel stiffness  $k_p$  increases, not only does  $f_L$  get higher, but  $\Delta f$  also gets smaller. Hence, the parallel stiffness  $k_p$  has only detrimental effects, and it is best to set  $k_p$  to zero to achieve both design objectives of lower gap frequency and larger gap size.

Therefore, the optimal design requires that the inerter has very large inertance and very stiff connections with the base structure, and it is better *not* to incorporate any stiffness parallel to the inerter. Because it is possible to fabricate inerters with inertance more than a million times of its actual mass ( $\mu_b \sim 10^6$ ) [47], the embedded inerter design shown in Fig. 2(b) is practical for engineering applications.

Next, we study an alternative metamaterial design with embedded mass-inerter resonators, as illustrated in Fig. 4(a). One end of the inerter is connected to the main chain, while the other end is connected to a resonator mass  $m$ . This results in a model with three degrees of freedom in each unit cell:  $u^M$  - displacement of mass  $M$  on the main chain,  $u^b$  - displacement of the point between stiffness  $k_b$  and inerter  $b$ , and  $u^m$  - displacement of the resonator mass  $m$ . Applying the same Bloch-wave procedures as before yields the dispersion bands for this system [38]. At the limit of large inertance ( $\mu_b \gg \mu_m, \kappa_b, \kappa_f$ ) and low frequency ( $f \ll 1$ ), we arrive at

$$f_L \rightarrow \frac{1}{2\pi} \sqrt{\frac{\kappa_b \kappa_m}{\mu_b (\kappa_b + \kappa_m)}} \quad \text{and} \quad \Delta f \rightarrow 0, \quad (7)$$

where  $\mu_b = b/M$ ,  $\mu_m = m/M$ ,  $\kappa_b = k_b/K$ , and  $\kappa_f = k_f/K$ . Since increasing the inertance closes the band gap ( $\Delta f \rightarrow 0$ ), this mass-inerter-resonator design shown in Fig. 4(a) is not suitable to achieve ultra-low frequency band gaps.

Lastly, we also look into the traditional locally resonant metamaterials with embedded mass-resonators, as illustrated in Fig. 4(b). The discrete model has two degrees

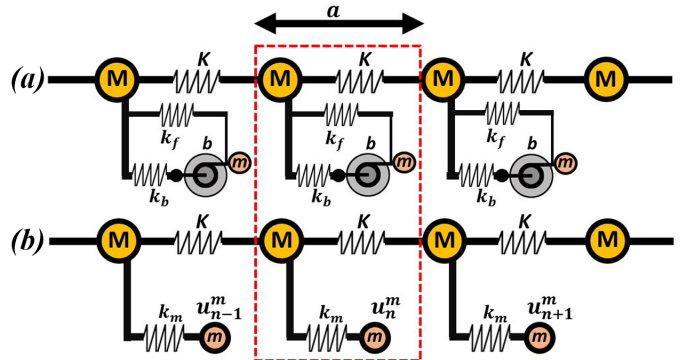


FIG. 4. Discrete models: (a) Metamaterial with inerter-mass-resonators; (b) Metamaterial with mass-resonators.

of freedom in each unit cell:  $u^M$  - displacement of mass  $M$  on the main chain, and  $u^m$  - displacement of the resonator mass  $m$ . The analytical closed-form expressions of the band gap edges are [38, 56]

$$f_L = \frac{1}{2\pi} \sqrt{\chi_m - \sqrt{\chi_m^2 - 4\frac{\kappa_m}{\mu_m}}}, \quad (8a)$$

$$f_U = \frac{1}{2\pi} \sqrt{\frac{\kappa_m}{\mu_m} + \kappa_m}, \quad (8b)$$

where  $\chi_m = \kappa_m/2 + \kappa_m/(2\mu_m) + 2$ ,  $\kappa_m = k_m/K$ , and  $\mu_m = m/M$ . Based on Eq. (8a), in order to achieve ultra-low-frequency band gaps with  $f_L \sim 10^{-4}$ , we need  $\mu_m/\kappa_m \sim 10^8$ . On the other hand, we need to avoid the case of  $\mu_m = m/M \gg 1$  since it would make the embedded mass-resonator too heavy as compared to the matrix material or base structure, and hence would be infeasible in most applications. The only viable choice is to adopt the ultra-low-stiffness design with  $\mu_m \sim 1$  and  $\kappa_m \ll 1$ , at which limit we get:

$$f_L \rightarrow \frac{1}{2\pi} \sqrt{\frac{\kappa_m}{\mu_m}} \quad \text{and} \quad \Delta f \rightarrow \sqrt{\mu_m + 1} - 1. \quad (9)$$

This approach to form a band gap at ultra-low frequencies may initially seem possible. In fact, with  $\mu_m = m/M = 1$  and  $\kappa_m = k_m/K = 5 \times 10^{-7}$ , we obtain exactly the same dispersion bands as those plotted in Fig. 2(c). However, in the same limit of  $\mu_m \sim 1$  and  $\kappa_m \ll 1$ , we get the modal displacement ratios at the gap edges as

$$\begin{aligned} U^b/U^M &\rightarrow 4/\kappa_m \quad \text{at} \quad f = f_L, \\ U^b/U^M &\rightarrow 1/\mu_m \quad \text{at} \quad f = f_U. \end{aligned} \quad (10)$$

Hence, the same design parameters give rise to a very high modal displacement ratio,  $U^b/U^M \rightarrow 4/\kappa_m = 8 \times 10^6$  at the lower gap edge  $f_L$  (marked with red square in Fig 2(c)). This means the resonator mass would vibrate with an amplitude that is millions of times of the vibration amplitude in the main chain. Therefore, the ultra-low stiffness design here is impractical in most application scenarios.

Based on the analyses of all three designs above, we conclude that the inerter-based metamaterial design depicted in Fig. 2(b) is the only suitable solution to achieve band gaps at the ultra-low dimensionless frequency of  $f = a/\lambda \sim 10^{-4}$  or lower.

To further demonstrate the efficacy and practicality of this design, we perform numerical studies on two-dimensional lattices with embedded inerters. Due to the close relevance to engineering applications, there have been many pioneering studies realizing band gaps in two- and three-dimensional metamaterials with other lever- or geometry-based inertial amplified structures [57–60], as well as two-dimensional structures that incorporate a flat plate [61–64] or a beam [50, 53, 65–69] as the base

structure with inerter-based resonators. However, none of the designs so far can achieve band gaps at the ultra-low dimensionless frequency of  $f = a/\lambda \sim 10^{-4}$ . In the following, we investigate the viable design illustrated in Fig. 2(b) in two-dimensional systems.

Here, we show conceptual two-dimensional designs in the form of inerter-in-lattice configurations that can represent various engineering structures. As shown in Fig. 5(a), for graphic compactness, we use a blue straight line to represent a connection with main-chain stiffness  $K$ , side-chain stiffness  $k_b$ , and side-chain inertance  $b$ . We assume the displacement  $u^b$  at the point between stiffness  $k_b$  and inerter  $b$  is always rigidly constrained in the lateral direction of the connection unit, so that  $u_b$  is always along the direction of the connection. Then, we construct square ( Fig. 5(b)) and triangular (Fig. 5(c)) lattices with this basic connection building block. All connections possess an embedded inerter on the side chain. Specifically for the square lattice, the diagonal connections are necessary to make the lattice statically stable, so that no zero-frequency band can exist. The crossing point of the two diagonal connections at the center of each square is not a joint, and there is no interactions here between the two diagonal connections. Although the formulations and derivations [38] are more challenging than those for one-dimensional cases, we can still study the two-dimensional designs via numerical results. With stiffness ratio  $\kappa_b = kb/K = 1$  and inertance ratio  $\mu_b = b/M = 10^6$ , we plot the dispersion curves of square and triangular lattices with embedded inerters in Figs. 5(d) and 5(e), respectively. A band gap exists in both cases with the lower gap edge frequency of  $f_L = 1.125 \times 10^{-4}$  and the relative gap size of  $\Delta f \approx 41.4\%$ . Not only do the band gaps match each other in the two different lattices, but they also match the band gap of the one-dimensional configuration shown in Fig. 2(b). This shows that the analyses and conclusions on band gaps about one-dimensional models directly extend to higher dimensional scenarios, and the difference in lattice configurations has negligible impact on the ultra-low-frequency band gap. Conceptually, in the very long wavelength limit of  $\lambda \gg a$ , the unit-cell level geometries and small length-scale details have minimal influence on the metamaterial behavior in the low-frequency regime.

To conclude, our analytical and numerical analyses offer clear guidelines to design elastic metamaterials with an ultra-low-frequency band gap: Each unit cell needs an embedded inerter with both terminals connected to the base material; no additional resonator mass should be used; to achieve band gaps at lower frequency, higher inertance is needed; and, to achieve wider band gaps, stiffer connection between the inerter and the base material is needed. These insights provide actionable guidelines for future studies towards low-frequency vibration mitigation using metamaterials. Although this study is

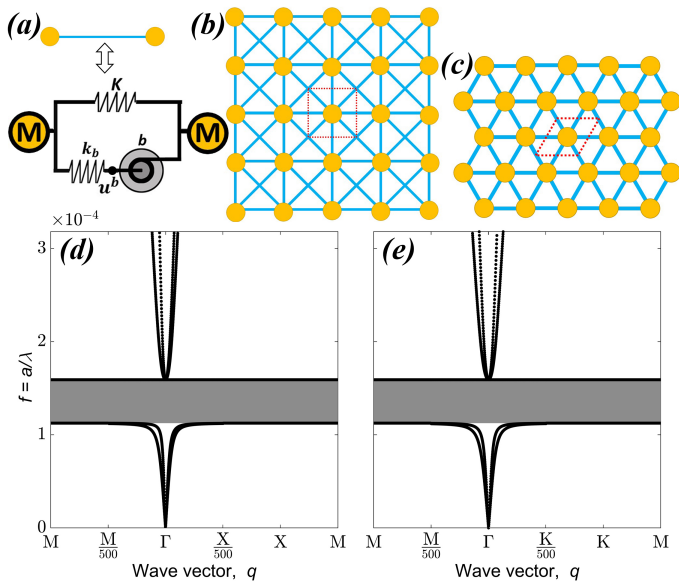


FIG. 5. Two-dimensional lattices with embedded inerters: (a) Basic connection unit used in both lattices. Note that  $u_b$  here is always just a single degree of freedom in any two-dimensional lattice, as we constrain it to allow displacement parallel to the connection only. (b) and (c) depict the square and triangular lattices with embedded inerters, respectively. With  $\kappa_b = k_b/K = 1$  and  $\mu_b = b/M = 10^6$ , (d) and (e) show the dispersion bands of configurations (b) and (c), respectively.

focused on periodic metamaterials, our analyses can be extended to quasi-crystalline [70–72], hyper-uniform [73–75], amorphous [76] or other non-periodic inerter-based metamaterial designs.

Both R.G.P and P.W. acknowledge the start-up research funds of the Department of Mechanical Engineering at University of Utah. The support and resources from the Center for High Performance Computing at the University of Utah are gratefully acknowledged. The authors thank Prof. Peter Zhu, Dr. Xiaolong Tong, Sharat Paul and Md Nahid Hasan for inspirational discussions.

[1] M. Maldovan and E. L. Thomas, *Periodic materials and interference lithography: for photonics, phononics and mechanics* (John Wiley & Sons, 2009).  
 [2] M. I. Hussein, M. J. Leamy, and M. Ruzzene, Dynamics of phononic materials and structures: Historical origins, recent progress, and future outlook, *Applied Mechanics Reviews* **66** (2014).  
 [3] D. Mu, H. Shu, L. Zhao, and S. An, A review of research on seismic metamaterials, *Advanced Engineering Materials* **22**, 1901148 (2020).  
 [4] L. Liu and H. P. Lee, A review: Elastic metamaterials and inverse design methods for shock and vibration mitigation, *International Journal of Applied Mechanics* **13**, 2150102 (2021).

[5] J. Ji, Q. Luo, and K. Ye, Vibration control based metamaterials and origami structures: A state-of-the-art review, *Mechanical Systems and Signal Processing* **161**, 107945 (2021).  
 [6] H. Laghfi and N. Lamdouar, Periodic structures as a countermeasure of traffic vibration and earthquake: A review, in *Advanced Technologies for Humanity*, edited by R. Saidi, B. El Bhiri, Y. Maleh, A. Mosallam, and M. Essaïdi (Springer International Publishing, Cham, 2022) pp. 359–373.  
 [7] S. Krodel, N. Thomé, and C. Daraio, Wide band-gap seismic metastructures, *Extreme Mechanics Letters* **4**, 111 (2015).  
 [8] Y. Achaoui, B. Ungureanu, S. Enoch, S. Brûlé, and S. Guenneau, Seismic waves damping with arrays of inertial resonators, *Extreme Mechanics Letters* **8**, 30 (2016).  
 [9] J. H. Oh, S. Qi, Y. Y. Kim, and B. Assouar, Elastic metamaterial insulator for broadband low-frequency flexural vibration shielding, *Physical Review Applied* **8**, 054034 (2017).  
 [10] X. Fang, J. Wen, B. Bonello, J. Yin, and D. Yu, Ultra-low and ultra-broad-band nonlinear acoustic metamaterials, *Nature Communications* **8**, 10.1038/s41467-017-00671-9 (2017).  
 [11] A. O. Krushynska, A. Amendola, F. Bosia, C. Daraio, N. M. Pugno, and F. Fraternali, Accordion-like metamaterials with tunable ultra-wide low-frequency band gaps, *New Journal of Physics* **20**, 073051 (2018).  
 [12] Muhammad, C. Lim, and J. Reddy, Built-up structural steel sections as seismic metamaterials for surface wave attenuation with low frequency wide bandgap in layered soil medium, *Engineering Structures* **188**, 440 (2019).  
 [13] Y. Chen, F. Qian, F. Scarpa, L. Zuo, and X. Zhuang, Harnessing multi-layered soil to design seismic metamaterials with ultralow frequency band gaps, *Materials and Design* **175**, 107813 (2019).  
 [14] L. D’Alessandro, R. Ardito, F. Braghin, and A. Corigliano, Low frequency 3d ultra-wide vibration attenuation via elastic metamaterial, *Scientific Reports* **9**, 10.1038/s41598-019-44507-6 (2019).  
 [15] P. Sun, Z. Zhang, H. Guo, N. Liu, and Y. Wang, Hierarchical square honeycomb metamaterials with low-frequency broad bandgaps and flat energy bands characteristics, *Journal of Applied Physics* **128**, 235102 (2020).  
 [16] Y. Zeng, P. Peng, Q.-J. Du, Y.-S. Wang, and B. Assouar, Subwavelength seismic metamaterial with an ultra-low frequency bandgap, *Journal of Applied Physics* **128**, 014901 (2020).  
 [17] Y. Ruan, X. Liang, X. Hua, C. Zhang, H. Xia, and C. Li, Isolating low-frequency vibration from power systems on a ship using spiral phononic crystals, *Ocean Engineering* **225**, 108804 (2021).  
 [18] D. Chen, H. Zi, Y. Li, and X. Li, Low frequency ship vibration isolation using the band gap concept of sandwich plate-type elastic metastructures, *Ocean Engineering* **235**, 109460 (2021).  
 [19] Q. Lin, J. Zhou, H. Pan, D. Xu, and G. Wen, Numerical and experimental investigations on tunable low-frequency locally resonant metamaterials, *Acta Mechanica Sinica* **34**, 612 (2021).  
 [20] M. Zhang, J. Yang, and R. Zhu, Origami-based bistable metastructures for low-frequency vibration control, *Journal of Applied Mechanics* **88**, 10.1115/1.4049953 (2021).  
 [21] Y. Huang and X. Zhang, Pentamode metamaterials with



- ultra-low-frequency single-mode band gap based on constituent materials, *Journal of Physics: Condensed Matter* **33**, 185703 (2021).
- [22] X. Wang, S. Wan, Y. Nian, P. Zhou, and Y. Zhu, Periodic in-filled pipes embedded in semi-infinite space as seismic metamaterials for filtering ultra-low-frequency surface waves, *Construction and Building Materials* **313**, 125498 (2021).
- [23] Muhammad and C. W. Lim, Phononic metastructures with ultrawide low frequency three-dimensional bandgaps as broadband low frequency filter, *Scientific Reports* **11**, 10.1038/s41598-021-86520-8 (2021).
- [24] W. Jiang, M. Yin, Q. Liao, L. Xie, and G. Yin, Three-dimensional single-phase elastic metamaterial for low-frequency and broadband vibration mitigation, *International Journal of Mechanical Sciences* **190**, 106023 (2021).
- [25] H.-F. Zhu, X.-W. Sun, T. Song, X.-D. Wen, X.-X. Liu, J.-S. Feng, and Z.-J. Liu, Tunable characteristics of low-frequency bandgaps in two-dimensional multivibrator phononic crystal plates under prestrain, *Scientific Reports* **11**, 10.1038/s41598-021-87904-6 (2021).
- [26] M. H. Bae, W. Choi, J. M. Ha, M. Kim, and H. M. Seung, Extremely low frequency wave localization via elastic foundation induced metamaterial with a spiral cavity, *Scientific Reports* **12**, 10.1038/s41598-022-08002-9 (2022).
- [27] Q. Li and M. Zhang, Elastic metamaterials of hexagonal unit cells with double-cone arms from pentamode to band gap at low frequencies, *Crystals* **12**, 10.3390/cryst12050604 (2022).
- [28] N. H. Vo, T. M. Pham, H. Hao, K. Bi, and W. Chen, A reinvestigation of the spring-mass model for metamaterial bandgap prediction, *International Journal of Mechanical Sciences* **221**, 107219 (2022).
- [29] H. Zi and Y. Li, Low-frequency broadband vibration attenuation of sandwich plate-type metastructures with periodic thin-wall tube cores, *Journal of Low Frequency Noise, Vibration and Active Control* **41**, 330 (2022).
- [30] Q. Lin, J. Zhou, K. Wang, D. Xu, G. Wen, Q. Wang, and C. Cai, Low-frequency locally resonant band gap of the two-dimensional quasi-zero-stiffness metamaterials, *International Journal of Mechanical Sciences* , 107230 (2022).
- [31] Y. Zeng, L. Cao, S. Wan, T. Guo, Y.-F. Wang, Q.-J. Du, B. Assouar, and Y.-S. Wang, Seismic metamaterials: Generating low-frequency bandgaps induced by inertial amplification, *International Journal of Mechanical Sciences* **221**, 107224 (2022).
- [32] Z. Yan, H. Xiao, Y. Liu, and T. Tan, Band-gap dynamics and programming for low-frequency broadband elastic metamaterial, *Composite Structures* , 115535 (2022).
- [33] M. M. Sigalas, Elastic and acoustic wave band structure, *Journal of sound and vibration* **158**, 377 (1992).
- [34] M. S. Kushwaha, P. Halevi, L. Dobrzynski, and B. Djafari-Rouhani, Acoustic band structure of periodic elastic composites, *Physical review letters* **71**, 2022 (1993).
- [35] Z. Liu, X. Zhang, Y. Mao, Y. Zhu, Z. Yang, C. T. Chan, and P. Sheng, Locally resonant sonic materials, *science* **289**, 1734 (2000).
- [36] P. Wang, F. Casadei, S. Shan, J. C. Weaver, and K. Bertoldi, Harnessing buckling to design tunable locally resonant acoustic metamaterials, *Physical review letters* **113**, 014301 (2014).
- [37] M. Z. Chen, C. Papageorgiou, F. Scheibe, F.-C. Wang, and M. C. Smith, The missing mechanical circuit element, *IEEE Circuits and Systems Magazine* **9**, 10 (2009).
- [38] See supplemental information at url for additional results, detailed derivations, and calculation procedures. the supplemental information cites refs. [1, 2, 36, 37, 39–47, 56, 77–84].
- [39] C. Papageorgiou and M. C. Smith, Laboratory experimental testing of inerters, in *Proceedings of the 44th IEEE Conference on Decision and Control* (IEEE, 2005) pp. 3351–3356.
- [40] C. Papageorgiou, N. E. Houghton, and M. C. Smith, Experimental testing and analysis of inerter devices, *Journal of dynamic systems, measurement, and control* **131** (2009).
- [41] Y. Shen, L. Chen, X. Yang, D. Shi, and J. Yang, Improved design of dynamic vibration absorber by using the inerter and its application in vehicle suspension, *Journal of Sound and Vibration* **361**, 148 (2016).
- [42] X. Sun, L. Chen, S. Wang, X. Zhang, and X. Yang, Performance investigation of vehicle suspension system with nonlinear ball-screw inerter, *International Journal of Automotive Technology* **17**, 399 (2016).
- [43] L. Yuehao, C. Zhe, H. Niaoqing, Y. Yi, and X. Zhuo, Modeling, design and experiments of a ball-screw inerter with mechanical diodes, *Journal of Sound and Vibration* **504**, 116121 (2021).
- [44] L. Yuehao, C. Zhe, H. Niaoqing, Y. Yi, and Y. Zhengyang, Study of dynamic breakdown of inerter and the improved design, *Mechanical Systems and Signal Processing* **167**, 108520 (2022).
- [45] R. Wang, X. Meng, D. Shi, X. Zhang, Y. Chen, and L. Chen, Design and test of vehicle suspension system with inerters, *Proceedings of the Institution of Mechanical Engineers, Part C: Journal of Mechanical Engineering Science* **228**, 2684 (2014).
- [46] F.-C. Wang, M.-F. Hong, and T.-C. Lin, Designing and testing a hydraulic inerter, *Proceedings of the Institution of Mechanical Engineers, Part C: Journal of Mechanical Engineering Science* **225**, 66 (2011).
- [47] S. Nakaminami, H. Kida, K. Ikago, and N. Inoue, Dynamic testing of a full-scale hydraulic inerter-damper for the seismic protection of civil structures, in *7th International Conference on Advances in Experimental Structural Engineering, AESE 2017* (Eucentre, 2017) pp. 41–54.
- [48] P. P. Kulkarni and J. M. Manimala, Longitudinal elastic wave propagation characteristics of inertant acoustic metamaterials, *Journal of Applied Physics* **119**, 245101 (2016).
- [49] H. Al Ba'ba'a, D. DePauw, T. Singh, and M. Nouh, Dispersion transitions and pole-zero characteristics of finite inertially amplified acoustic metamaterials, *Journal of Applied Physics* **123**, 105106 (2018).
- [50] X. Fang, K.-C. Chuang, X. Jin, and Z. Huang, Band-gap properties of elastic metamaterials with inerter-based dynamic vibration absorbers, *Journal of Applied Mechanics* **85**, 071010 (2018).
- [51] K. Madhamshetty and J. M. Manimala, Extraordinary wave manipulation characteristics of nonlinear inertant acoustic metamaterials, *Journal of the Franklin Institute* **356**, 7731 (2019).
- [52] F. Sun and L. Xiao, Bandgap characteristics and seismic

- applications of inerter-in-lattice metamaterials, *Journal of Engineering Mechanics* **145**, 04019067 (2019).
- [53] M. Cajić, J. Christensen, and S. Adhikari, Tuning of topological interface modes in an elastic beam array system with inerters, *International Journal of Mechanical Sciences* **205**, 106573 (2021).
- [54] Y. Liu, J. Yang, X. Yi, and D. Chronopoulos, Enhanced suppression of low-frequency vibration transmission in metamaterials with linear and nonlinear inerters, *Journal of Applied Physics* **131**, 105103 (2022).
- [55] M. Wang, F.-F. Sun, S. Nagarajaiah, and Y.-W. Li, Frequency-dependency/independency analysis of damping magnification effect provided by tuned inerter absorber and negative stiffness amplifying damper considering soil-structure interaction, *Mechanical Systems and Signal Processing* **172**, 108965 (2022).
- [56] H. Al Ba'ba'a, M. Nouh, and T. Singh, Formation of local resonance band gaps in finite acoustic metamaterials: A closed-form transfer function model, *Journal of Sound and Vibration* **410**, 429 (2017).
- [57] G. Acar and C. Yilmaz, Experimental and numerical evidence for the existence of wide and deep phononic gaps induced by inertial amplification in two-dimensional solid structures, *Journal of Sound and Vibration* **332**, 6389 (2013).
- [58] S. Taniker and C. Yilmaz, Design, analysis and experimental investigation of three-dimensional structures with inertial amplification induced vibration stop bands, *International Journal of Solids and Structures* **72**, 88 (2015).
- [59] R. Zaccherini, A. Colombi, A. Palermo, H. R. Thomsen, and E. N. Chatzi, Stress-optimized inertial amplified metastructure with opposite chirality for vibration attenuation, arXiv preprint arXiv:2111.08594 (2021).
- [60] R. Zaccherini, *Granular Metasurfaces and Inertial Amplified Metastructures for Vibration Attenuation*, Ph.D. thesis, ETH Zurich (2021).
- [61] A. F. Russillo, G. Failla, and G. Alotta, Ultra-wide low-frequency band gap in locally-resonant plates with tunable inerter-based resonators, *Applied Mathematical Modelling* **106**, 682 (2022).
- [62] T. Wang, Tunable band gaps in an inertant metamaterial plate with two-degree-of-freedom local resonance, *Physics Letters A* **384**, 126420 (2020).
- [63] J. Li, P. Yang, and S. Li, Reduction of sound transmission through finite clamped metamaterial-based double-wall sandwich plates with poroelastic cores, *Acta Acustica united with Acustica* **105**, 850 (2019).
- [64] T. Wang, J. Liu, and M. Chen, Sound transmission loss of an inertant metamaterial plate submerged in moving fluids, *Applied Mathematical Modelling* (2022).
- [65] X. Fang, K.-C. Chuang, X.-L. Jin, D.-F. Wang, and Z.-L. Huang, An inertant elastic metamaterial plate with extra wide low-frequency flexural band gaps, *Journal of Applied Mechanics* **88** (2021).
- [66] Z. Dong, D. Chronopoulos, and J. Yang, Enhancement of wave damping for metamaterial beam structures with embedded inerter-based configurations, *Applied Acoustics* **178**, 108013 (2021).
- [67] L. Zhou, W. Han, and S. Wan, Low frequency band gap for box girder attached idvas, *Thin-Walled Structures* **174**, 109088 (2022).
- [68] Z. Dong, J. Yang, C. Zhu, D. Chronopoulos, and T. Li, Energy flow and performance evaluation of inerter-based vibration isolators mounted on finite and infinite flexible foundation structures, *Advances in Mechanical Engineering* **14**, 16878140211070461 (2022).
- [69] A. Aladwani, A. Mohammed, and M. Nouh, Tunable dissipation in elastic metamaterials via methodic reconfiguration of inertant mechanical networks, *Meccanica*, 1 (2022).
- [70] M. I. N. Rosa, Y. Guo, and M. Ruzzene, Exploring topology of 1d quasiperiodic metastructures through modulated LEGO resonators, *Applied Physics Letters* **118**, 131901 (2021).
- [71] R. L. Thomes, J. A. Mosquera-Sánchez, and C. D. Marqui, Bandgap widening by optimized disorder in one-dimensional locally resonant piezoelectric metamaterials, *Journal of Sound and Vibration* **512**, 116369 (2021).
- [72] Y. Liu, L. F. Santos, and E. Prodan, Topological gaps in quasiperiodic spin chains: A numerical and k-theoretic analysis, *Physical Review B* **105**, 035115 (2022).
- [73] G. Gkantounis, T. Amoah, and M. Florescu, Hyperuniform disordered phononic structures, *Physical Review B* **95**, 094120 (2017).
- [74] V. Romero-García, É. Chéron, S. Kuznetsova, J.-P. Groby, S. Félix, V. Pagneux, and L. M. García-Raffi, Wave transport in 1d stealthy hyperuniform phononic materials made of non-resonant and resonant scatterers, *APL Materials* **9**, 101101 (2021).
- [75] S. M. Kuznetsova, J.-P. Groby, L. M. García-Raffi, and V. Romero-García, Localized interface modes in one-dimensional hyperuniform acoustic materials, *Journal of Physics D: Applied Physics* **54**, 315303 (2021).
- [76] N. P. Mitchell, L. M. Nash, D. Hexner, A. M. Turner, and W. Irvine, Amorphous topological insulators constructed from random point sets, *Nature Physics* **14**, 380 (2018).
- [77] S. El-Borgi, R. Fernandes, P. Rajendran, R. Yazbeck, J. Boyd, and D. Lagoudas, Multiple bandgap formation in a locally resonant linear metamaterial beam: Theory and experiments, *Journal of Sound and Vibration* **488**, 115647 (2020).
- [78] E. Ghavanloo, S. A. Fazelzadeh, and H. Raffi-Tabar, Formulation of an efficient continuum mechanics-based model to study wave propagation in one-dimensional diatomic lattices, *Mechanics Research Communications* **103**, 103467 (2020).
- [79] M. Owaidat, Determination of the vibrational frequencies of the decorated triangular and centered triangular lattices, *The European Physical Journal Plus* **135**, 1 (2020).
- [80] K. Saito and N. Inoue, A study on optimum response control of passive control systems using viscous damper with inertial masssubstituting equivalent nonlinear viscous elements for linear viscous elements in optimum control systems, *AIJ Journal of Technology and Design* **13** (2007).
- [81] M. C. Smith, Synthesis of mechanical networks: the inerter, *IEEE Transactions on automatic control* **47**, 1648 (2002).
- [82] A. L. Stanford and J. M. Tanner, *Physics for students of science and engineering* (Academic Press, 2014).
- [83] X. Xu, M. V. Barnhart, X. Li, Y. Chen, and G. Huang, Tailoring vibration suppression bands with hierarchical metamaterials containing local resonators, *Journal of Sound and Vibration* **442**, 237 (2019).
- [84] Y. Liu, X. An, H. Chen, and H. Fan, Vibration attenuation of finite-size metaconcrete: Mechanism, prediction and verification, *Composites Part A: Applied Science and*

Manufacturing **143**, 106294 (2021).